Posterodorsal medial amygdala urocortin-3, GABA and glutamate mediate suppression of LH pulsatility in female mice

Deyana Ivanova[1], Xiao-Feng Li[1], Caitlin McIntyre[1] and Kevin T O'Byrne[1]

[1]Department of Women and Children's Health, School of Life Course and Population Sciences, Faculty of Life Science and Medicine, King's College London, UK

Short title: MePD Ucn3 effect on LH and corticosterone release

Key words: Ucn3, GABA, glutamate, MePD, PVN, LH pulsatility, CORT secretion

Corresponding author's contact details: Deyana Ivanova (deyana.ivanova@kcl.ac.uk) and Kevin T O'Byrne (kevin.obyrne@kcl.ac.uk), Department of Women and Children's Health, School of Life Course and Population Sciences, Faculty of Life Science and Medicine, King's College London, 2.92W Hodgkin Building, Guy's Campus, London SE1 1UL, UK.

Reprint requests: Deyana Ivanova, Department of Women and Children's Health, School of Life Course Sciences, Faculty of Life Science and Medicine, King's College London, 2.92W Hodgkin Building, Guy's Campus, London SE1 1UL, UK.

Grants supporting paper: UKRI: BBSRC (BB/S000550/1 & BB/W005913/1). DI is a PhD student funded by MRC-DTP studentship.

The authors have nothing to disclose.

Abstract

The posterodorsal subnucleus of the medial amygdala (MePD) is an upstream modulator of the hypothalamic-pituitary-gonadal (HPG) and hypothalamic-pituitary-adrenal (HPA) axes. Inhibition of MePD urocortin-3 (Ucn3) neurons prevents psychological stress-induced suppression of LH pulsatility while blocking the stress-induced elevations in corticosterone (CORT) secretion in female mice. We explore the neurotransmission and neural circuitry suppressing the GnRH pulse generator by MePD Ucn3 neurons and we further investigate whether MePD Ucn3 efferent projections to the PVN control CORT secretion and LH pulsatility. Ucn3-cre-tdTomato female ovariectomised (OVX) mice were unilaterally injected with AAV-ChR2 and implanted with optofluid cannulae targeting the MePD. We optically activated Ucn3 neurons in the MePD with blue light at 10Hz and monitored the effect on LH pulses. Next, we combined optogenetic stimulation of MePD Ucn3 neurons with pharmacological antagonism of $GABA_A$ or $GABA_B$ receptors with bicuculline or CGP, respectively, as well as a combination of NMDA and AMPA receptor antagonists, AP5 and CNQX respectively, and observed the effect on pulsatile LH secretion. A separate group of Ucn3-cre-tdTomato OVX mice with 17ß-estradiol (E_2) replacement were unilaterally injected with AAV-ChR2 in the MePD and implanted with fibreoptic cannulae targeting the PVN. We optically stimulated the MePD Ucn3 efferent projections in the PVN with blue light at 20Hz and monitored the effect on CORT secretion and LH pulses. We reveal for the first time that activation of Ucn3 neurons in the MePD inhibits GnRH pulse generator frequency via GABA and glutamate signalling within the MePD, while MePD Ucn3 projections to the PVN modulate the HPG and HPA axes.

Introduction

Stress exerts a profound suppressive effect on reproduction in mammals, including rodents and humans. The amygdala, part of the limbic system, is a key emotional centre integrating incoming cues from the external environment, such as anxiogenic signals, with the reproductive and stress axes (1). The posterodorsal sub-nucleus of the medial amygdala (MePD) is an upstream modulator of pulsatile luteinizing hormone (LH) secretion (2–4) and exerts an inhibitory break on pubertal timing (5,6). The MePD sends direct projections, of an unknown phenotype, to the kisspeptin (kiss1) neuronal population in the hypothalamic arcuate nucleus (ARC) (7,8) known as KNDy because they co-express neurokinin B (NKB) and dynorphin A (Dyn) (9–11). The synchronous activity of the ARC KNDy network drives pulsatile gonadotropin-releasing hormone (GnRH) and LH release (11–14). The MePD also contains a kiss1 neuronal population and selective optogenetic activation of these neurons increases GnRH pulse generator frequency in mice (4) and unpublished observations show this is an effect involving both MePD GABA and glutamate signalling.

We have recently shown that urocortin-3 (Ucn3), a member of the corticotropin-releasing factor (CRF) stress neuropeptide family, and its receptor CRF type 2 (CRFR2) signalling in the MePD are involved in mediating the suppressive effect of psychosocial stress on LH pulsatility (3). However, the underlying neural mechanisms involved in mediating the inhibitory effect of MePD Ucn3 neurons on LH pulsatility remain to be established. GABA and glutamate signalling in the amygdala are implicated in the modulation of anxiety behaviour (15,16). The amygdala also modulates the stress response through the hypothalamic pituitary adrenal (HPA) axis. The medial amygdala activates the HPA axis in response to predator odor stress (17) and the MePD in particular has been shown to send stress-activated efferents to the paraventricular nucleus of hypothalamus (PVN) (18). Furthermore, MePD Ucn3 and CRFR2-positive neurons are implicated in regulating the stress response, with restraint stress increasing

65 MePD Ucn3 (19) and social defeat elevating MePD CRFR2 expression in rodents (20).
66 Moreover, MePD Ucn3 and CRFR2-positive neurons project to the PVN (21), and we have
67 recently shown that chemogenetic inhibition of MePD Ucn3 neurons prevents psychogenic
68 stress-induced corticosterone (CORT) release in female mice (3).

69 In this study, we aimed to determine whether activation of MePD Ucn3 neurons inhibits
70 pulsatile LH secretion via GABA and or glutamate signalling within this amygdala sub-
71 nucleus. To achieve this, we will combine selective optogenetic activation of MePD Ucn3
72 neurons with pharmacological antagonism of $GABA_A$ or $GABA_B$ receptors, or a combination
73 of N-methyl-D-aspartate (NMDA) and α-amino-3-hydroxy-5-methyl-4-isoxazole propionic
74 acid (AMPA) receptors, respectively, using chronically implanted intra-MePD optofluid
75 cannulae while collecting serial blood samples for LH pulse measurement in Ucn3-Cre-
76 tdTomato female mice. Additionally, we will investigate whether optogenetic stimulation of
77 MePD Ucn3 projection terminals in the PVN induce CORT release and suppress LH pulsatility.

78 **Methods**

79 **Mice**

80 Cryopreserved sperm of Ucn3-cre mice (strain Tg(Ucn3-cre)KF43Gsat/Mmucd; congenic on
81 C57BL/6 background) was acquired from MMRRC GENSAT and heterozygous transgenic
82 breeding pairs of Ucn3-Cre mice were recovered via insemination of female C57Bl6/J mice at
83 King's College London, as described previously (3). Ucn3-Cre mice were genotyped using
84 PCR for the detection of heterozygosity and Ucn3-cre mice were bred with td-Tomato mice
85 (strain B6.Cg-Gt(ROSA)26Sortm9(CAG-tdTomato)Hze/J; congenic on C57BL/6
86 background) acquired from The Jackson Laboratory, Bar Harbor, ME, USA to produce Ucn3-
87 cre-tdTomato reporter mice, as described previously (3,21). Female Ucn3-cre-tdTomato mice

88 weighing 19-23 g and aged 6-8 weeks were singly housed in individually ventilated cages
89 sealed with a HEPA-filter at 25 ± 1 °C in a 12:12 h light/dark cycle, lights on at 07:00 h
90 equipped with nesting material, wood-chip bedding and food and water ad libitum. All
91 procedures were carried out following the United Kingdom Home Office Regulations and
92 approved by the Animal Welfare and Ethical Review Body Committee at King's College
93 London.

94 **Stereotaxic injection of adeno-associated-virus carrying the channelrhodopsin construct**
95 **and fibre optic or optofluid cannula implantation**

96 All surgical procedures were carried out under aseptic conditions with general anaesthesia
97 using ketamine (Vetalar, 100 mg/kg, i.p.; Pfizer, Sandwich, UK) and xylazine (Rompun, 10
98 mg/kg, i.p.; Bayer, Leverkusen, Germany). Ucn3-Cre-tdTomato mice were secured in a David
99 Kopf stereotaxic frame (Kopf Instruments, Model 900) and either solely bilaterally
100 ovariectomised (OVX) or implanted with an 17ß-estradiol (E_2) silastic capsule. E_2 was
101 dissolved in sesame oil to reach a final concentration of 36 µg E_2/mL and filled in 14 mm
102 capsules of inner/outer diameter: 1.575/3.175 mm, as previously described (22). The reference
103 study reported that at 21 days of implantation, serum E_2 concentrations were within
104 physiological concentrations equivalent to those found in mice in the diestrous stage of the
105 cycle. However, by 35 days of implantation the serum E_2 concentrations had slowly declined
106 but still within the range found in diestrous mice. Due to the technically demanding nature of
107 our experiments the E_2 capsules were implanted for longer than 35 days post-surgery during
108 the experimental period. Therefore, E_2 levels may be lower than expected for the diestrous
109 phase. E_2 is known to enhance the suppressive effects of stress where the action of the gonadal
110 steroids sensitizes the HPA axis and augments stress-induced inhibition of the GnRH pulse
111 generator in many species, from rodents to primates (42–45). We had two experimental

112 groups; OVX only and OVX + E_2 capsule. The mouse brain atlas of Paxinos and Franklin (23)
113 was used to obtain target coordinates for the MePD (2.30 mm lateral, -1.55 mm from bregma,
114 at a depth of -4.94 mm below the skull surface). To reveal the skull an incision was made of
115 the scalp and one small hole was drilled above the location of the right MePD. AAV9-EF1a-
116 double floxed-hChR2(H134R)-EYFP-WPRE-HGHpA (300 nL; $3x10^{11}$ GC/ml; Serotype:9;
117 Addgene, Massachusetts, USA) was unilaterally injected into the right MePD using a 2-µL
118 Hamilton micro syringe (Esslab, Essex, UK) over 10 min, using the robot stereotaxic system
119 (Neurostar, Tubingen, Germany), performed for the targeted expression of ChR2-EYFP in
120 MePD Ucn3 neurons. After injection, the needle was left in position for a further 5 min and
121 lifted slowly over 2 min. Cre-positive mice received the AAV-ChR2 injection (test mice) or a
122 control virus AAV-YFP (Addgene) (control mice). The control virus does not contain the
123 ChR2 construct. The mice were then implanted with a dual optofluid cannula (Doric Lenses,
124 Quebec, Canada) at the same AP and ML coordinates as the viral injection site, however a
125 different DV was used such that the internal cannula targets the MePD and the fibre optic
126 cannula is situated 0.2 mm above the MePD site. Once in position the optofluid cannula was
127 secured on the skull using dental cement (Super-Bond Universal Kit, Prestige Dental, UK) and
128 the incision of the skin was closed with suture. Mice were left to recover for one week and
129 after recovery period, mice were handled daily to acclimatise to experimental procedures for a
130 further 2 weeks. Thirteen mice received the AAV-ChR2 injection and were implanted with an
131 optofluid cannula in the MePD. Five mice received the control AAV-YFP and were implanted
132 with an optofluid cannula in the MePD. Eleven mice received the AAV-ChR2 injection in the
133 MePD and were implanted with an optic fibre in the PVN. Five mice received the control
134 AAV-YFP and were implanted with an optic fibre in the PVN.

135 **In vivo optogenetic stimulation of MePD Urocortin-3 neurons**

136 In order to test the effect of optogenetic stimulation of MePD Ucn3 neurons on LH pulsatility
137 the ferrule of the implanted optofluid cannula, on the right side of the MePD, was attached via
138 a ceramic mating sleeve to a multimode fibre optic rotatory joint patch cable (Thorlabs LTD,
139 Ely, UK) at a length allowing for free movement of the mouse in their cage and blue light (473
140 nm wavelength; 10 mW) was delivered using a Grass SD9B stimulator-controlled laser
141 (Laserglow Technologies, Toronto, Canada). The mice were left to acclimatise for 1 h.
142 Following the acclimatisation period blood samples (5 μL) were collected every 5 min for 2 h
143 where after 1 h of control blood sampling, Ucn3-cre-tdTomato mice received optic stimulation
144 at 10 Hz with a 10 ms pulse interval and pattern stimulation of 5 seconds on and 5 seconds off
145 for the remaining 1 h.

146 **Intra-MePD administration of bicuculline (BIC), CGP-35348 or AP5 + CNQX during**
147 **optogenetic stimulation of MePD Urocortin-3 neurons**

148 Neuropharmacological manipulation of GABA and glutamate receptor signalling in the MePD
149 with or without optogenetic stimulation of MePD Ucn3 neurons was done to test whether
150 MePD Ucn3 induced suppression of LH pulsatility involves GABA or glutamate receptor
151 signalling. OVX mice implanted with a optofluid cannula in the MePD were subjected to the
152 tail-tip blood collection procedure, as previously described (24). Infusion of drugs with or
153 without optogenetic stimulation and blood sampling were performed between 09:00-13:00 h,
154 where 5 μl blood was collected every 5 min for 2 h. Internal cannula (Doric Lenses) attached
155 to extension tubing (0.58 mm ID, 0.96 mm OD), preloaded with bicuculline (BIC) ($GABA_A$
156 receptor antagonist; Sigma-Aldrich), CGP-35348 ($GABA_B$ receptor antagonist; Sigma-
157 Aldrich), AP5 + CNQX cocktail (NMDA and AMPA receptor antagonists; Tocris) or aCSF as
158 vehicle control, was inserted into the guide cannula of the optofluid implant and mice were
159 connected to the laser as described above. The tubing for drug infusion extended beyond the

160 cage and the distal ends were attached to 10-µl Hamilton syringes (Waters Ltd, Elstress, UK)
161 fitted into a PHD 2000 Programmable syringe pump (Harvard Apparatus, Massachusetts,
162 USA), allowing for a continuous infusion of the drug at a constant rate and mice were kept in
163 the cage throughout the experiment, freely-moving with food and water *ad libitum*. After 55
164 min of control blood sampling, the mice were given an initial bolus injection, 0.30 µl at a rate
165 of 0.06 µl/min over 5 min, of BIC, CGP-35348, AP5 + CNQX or aCSF. The laser was turned
166 on at 60 min and the bolus injection was followed by a continuous infusion, 0.8 µl at a rate of
167 0.01 µl/min over 1 h, of BIC, CGP-35348, AP5 + CNQX or aCSF. BIC, CGP-35348, AP5 and
168 CNQX were dissolved in aCSF to reach bolus concentrations of 20 pmol, 4.5 nmol, 1.2 nmol
169 and 0.5 nmol respectively. The concentrations for the continuous infusion of BIC, CGP-35348,
170 AP5 and CNQX were 68 pmol, 15 nmol, 2nmol and 1 nmol respectively. In the absence of
171 optic stimulation, the same regimen was applied. Data collection was conducted over a period
172 of 4-6 weeks. The mice receive all treatments in a random order, with at least 2 days between
173 experiments.

174 **MePD Urocortin-3 terminal optogenetic stimulation in the PVN**

175 To test the effect of optogenetic stimulation of MePD Ucn3 neuronal terminals in the PVN on
176 LH pulsatility and CORT release, OVX + E_2 Ucn3-cre-tdTomato mice with AAV-ChR2
177 injection in the right MePD implanted with a fibre optic cannula in the right PVN were
178 subjected to the tail-tip blood collection procedure, as previously described (24). For LH
179 measurement, blood samples were collected every 5 min for 2 h, as described above. Mice
180 were connected to the laser as described above. Optogenetic stimulation was initiated after the
181 1 h control blood sampling period and Ucn3-cre-tdTomato mice received optic stimulation at
182 20 Hz, 15 mW with a 10 ms pulse interval and pattern stimulation of 5 seconds on and 5
183 seconds off for the remaining 1 h. For CORT measurements, 15 µl blood samples were

184 collected on a separate occasion and blood samples were stored in tubes containing 5 µl
185 heparinised saline (5 IU ml^{-1}). Optogenetic stimulation was initiated, as described above, 30
186 min into the experiment (time point, 0 min) and lasted for 1 h (time point 60 min). Remaining
187 blood samples were collected at 0, 30 and 60 min, with a final sample taken 1 h after the
188 termination of optogenetic stimulation (time point, 120 min). At the end of the experiment,
189 blood samples were centrifuged at 13,000 RPM for 20 min at 20°C and plasma stored at -20°C.
190 Data collection was conducted over a period of 4-6 weeks. All experiments were performed
191 between 9:00-12:00 h.

192 **Validation of AAV injection and cannula implant site**

193 Upon completion of experiments, mice were anaesthetised with a lethal dose of ketamine and
194 transcardial perfusion was performed with heparinised saline for 5 min followed by ice-cold
195 4% paraformaldehyde (PFA) in phosphate buffer (pH 7.4) for 15 min using a pump (Minipuls,
196 Gilson, Villiers Le Bel, France). Mice brains were collected immediately and post-fixed in
197 15% sucrose in 4% PFA at 4 °C and left to sink. Once sunk, they were transferred to 30%
198 sucrose in phosphate-buffered saline (PBS) and left to sink. Brains were snap-frozen in
199 isopropanol on dry ice and stored in -80°C until further processing. Every third coronal brain
200 section (30-µm/section) through-out the MePD region (-1.34 mm to -2.70 mm from bregma)
201 was collected using a cryostat (Bright Instrument Co., Luton, UK). Sections were mounted on
202 microscope slides, air dried and covered with ProLong Antifade mounting medium (Molecular
203 Probes, Inc. OR, USA). Cannula placement and AAV injection site was verified with
204 Axioskop 2 Plus microscope equipped with Axiovision, version 4.7 (Zeiss) by determining
205 whether cannula reach the MePD. For AAV-ChR2-EYFP injected Ucn3-cre-tdTomato mice
206 we determined whether Ucn3 neurons were infected in the MePD region by merging td-Tomato
207 fluorescence of Ucn3 neurons with YFP fluorescence in the MePD. The number of Ucn3

208 mCitrine-positive neurones co-localised with td-Tomato fluorescence in the MePD of each
209 animal was counted using 4 sections and the average number of neurons presented is per section
210 per MePD. The group mean percent was calculated by taking the average number of Ucn3
211 mCitrine-positive neurons out of the average number of Ucn3 neurons expressing td-Tomato
212 fluorescence per 4 sections and presented as mean ± SEM %, as described previously (3).
213 Axioskop 2 Plus microscope (Carl Zeiss) equipped with axiovision, version 4.7 (Carl Zeiss)
214 was used to take images. Only mice with correct AAV injection and cannula placement in the
215 MePD were analysed.

216 **LH and CORT measurement**

217 Mice were handled daily to acclimatise to the tail-tip blood sampling procedure for LH
218 measurement (3). Blood samples collected for LH measurement were processed using LH
219 ELISA, as previously reported (3). The capture antibody (monoclonal antibody, anti-bovine
220 LHβ subunit, AB_2665514) was purchased from Department of Animal Science at the
221 University of California, Davis. The mouse LH standard (AFP-5306A) and primary antibody
222 (polyclonal antibody, rabbit LH antiserum, AB_2665533) were obtained from Harbour-UCLA
223 (California, USA). The secondary antibody (Horseradish-Peroxidase (HRP)-linked donkey
224 anti-rabbit IgG polyclonal antibody, AB_772206) was purchased from VWR International
225 (Leicestershire, UK). Intra-assay and inter-assay variations were 4.6% and 10.2%, respectively
226 and the assay sensitivity was 0.0015 ng/mL. DynPeak algorithm was used for the detection of
227 LH pulses (3). The effect of optogenetic stimulation of MePD Ucn3 neurons and
228 neuropharmacology studies was established by comparing the LH inter-pulse interval (IPI)
229 from the 1 h control period (pre-stimulation) or drug administration control period to the 1 h
230 experimental period, as previously described (3). The LH pulse amplitude was calculated as
231 the difference between the peak of an LH pulse and the baseline LH level before the onset of
232 the pulse. The means were compared between the pre-treatment and treatment periods for all

233 experiments. The LH pulse amplitude was also compared between experimental groups within
234 the treatment period. The mean LH value for each LH pulse profile was quantified by summing
235 all values from one LH pulse profile and dividing by the number of values recorded in 120
236 mins.

237 Blood samples were collected for CORT measurement were processed using a commercially
238 available enzyme immunoassay (EIA) kit (sheep polyclonal antibody specific for
239 corticosterone, AB_2877626; DetectX® Corticosterone Enzyme Immunoassay Kit, K014;
240 Arbor Assays, Michigan, USA), as described previously (3).

241 **Statistics**

242 Mice were compared between groups using a two-way ANOVA with a Tukey post-hoc and
243 data was presented as mean ± SEM. Statistics were performed using Igor Pro 7, Wavemetrics,
244 Lake Oswego, OR, USA. Data was represented as mean ± SEM and +$p<0.05$, ++$p<0.001$ and
245 +++$p<0.0001$ were considered to be significant.

246 **Results**

247 **Effects of optogenetic stimulation of MePD Urocortin-3 neurons on LH pulse frequency**

248 Optogenetic stimulation of MePD Ucn3 neurons in control mice had no effect on LH pulse
249 interval (Fig. 1A; AAV-YFP: n = 3) and administration of aCSF alone (AAV-YFP with no
250 stimulation: n = 2) had no effect on LH pulse interval. Optogenetic stimulation of MePD Ucn3
251 neurons with blue light at 10 Hz, 10 mW suppressed pulsatile LH secretion (Fig. 1B; AAV-
252 ChR2: n = 9). These data are summarized in the figure 1C. LH pulse amplitude was quantified
253 and data is provided in supplemental table (25).

254 **Effects of intra-MePD administration of bicuculline (BIC), a $GABA_AR$ antagonist, and**
255 **CGP, a $GABA_BR$ antagonist, during optical stimulation of MePD Urocortin-3 neurons**
256 **on LH pulsatility**

257 Delivery of BIC alone had no significant effect on LH pulsatility (Fig. 1D; n = 8). Intra-MePD
258 infusion of BIC during optogenetic stimulation of MePD Ucn3 neurons with blue light at 10
259 Hz, 10 mW completely blocked the suppressive effect of MePD Ucn3 neuronal activation on
260 LH pulsatility (Fig. 1E; n = 9). The results of this experiment are summarised in the figure 1F.
261 LH pulse amplitude was quantified and data is provided in supplemental table (25).

262 **Effects of intra-MePD administration of CGP, a $GABA_BR$ antagonist, during optical**
263 **stimulation of MePD Urocortin-3 neurons on LH pulsatility**

264 Delivery of CGP alone had no significant effect on LH pulsatility (Fig. 1G; n = 7). Intra-MePD
265 infusion of CGP during optogenetic stimulation of MePD Ucn3 neurons with blue light at 10
266 Hz, 10 mW completely blocked the suppressive effect of MePD Ucn3 neuronal activation on
267 LH pulsatility (Fig. 1H; n = 7). The results of this experiment are summarised in the figure 1I.
268 LH pulse amplitude was quantified and data is provided in supplemental table (25).

269 **Effects of intra-MePD glutamate antagonism during optogenetic stimulation of MePD**
270 **Urocortin-3 neurons on LH pulsatility**

271 Delivery of AP5 + CNQX alone had no significant effect on LH pulsatility (Fig. 1J; n = 6).
272 Intra-MePD infusion of AP5 (selective NMDA antagonist) + CNQX (selective AMPA
273 antagonist) during optogenetic stimulation of MePD Ucn3 neurons with blue light at 10 Hz, 10
274 mW completely blocked the suppressive effect of MePD Ucn3 neuronal activation on LH
275 pulsatility (Fig. 1K; n = 6). The results of this experiment are summarised in the figure 1L.
276 LH pulse amplitude was quantified and data is provided in supplemental table (25).

277 **Effect of MePD Urocortin-3 terminal stimulation in the PVN on dynamic CORT secretion**

278 Optogenetic stimulation of MePD Ucn3 neuron terminals in the PVN with blue light at 20 Hz,
279 15 mW elevated CORT secretion compared to controls (Fig. 2; AAV-ChR2: n = 6).
280 Optogenetic stimulation of MePD Ucn3 neurons and terminal projections in the PVN in control
281 mice had no effect on dynamic CORT secretion (AAV-YFP; n = 5).

282 **Effect of MePD Urocortin-3 terminal stimulation in the PVN on LH pulsatility**

283 Optogenetic stimulation of MePD Ucn3 projections in the PVN in control mice had no effect
284 on LH pulse interval (Fig. 3A and C; AAV-YFP, n = 3; wild-type with AAV-ChR2, n = 2) and
285 no stimulation of the MePD Ucn3 projections in the PVN (no stimulation, n = 2) had no effect
286 on LH pulse interval. Optogenetic stimulation of MePD Ucn3 neuron terminals in the PVN
287 with blue light at 20 Hz, 15 mW reduced LH pulsatility compared to controls (Fig. 3B and D;
288 AAV-ChR2: n = 8). These data are summarised in the figure 3E. LH pulse amplitude was
289 quantified and data is provided in supplemental table (25).

290 **Selective expression of ChR2 in MePD Ucn3 neurons and MePD Ucn3 neuron**
291 **projections in the PVN, and validation of cannula position**

292 Evaluation of AAV9-EF1a-double floxed-hChR2(H134R)-EYFP-WPRE-HGHpA expression
293 in tdTomato labelled neurons from AAV-injected Ucn3-cre-tdTomato mice revealed that 87.00
294 ± 6.00% of MePD Ucn3 neurons expressed AAV-ChR2 and the number of tdTomato labelled
295 Ucn3 neurons per side per slice in the MePD was counted at 49.00 ± 5.37 (mean ± SEM) with
296 the number of AAV-ChR2 infected neurons being 43.01 ± 3.65 (mean ± SEM) (n=8). Non-
297 specific expression of ChR2 in the MePD (YFP single labelling) has been quantified to be
298 limited to 6 ± 4.63 (mean ± SEM) in all of 8 mice. A representative example is shown in figure
299 4, A-F. The optofluid cannula was also verified to be correctly positioned in the MePD in all

300 of 8 mice. Evaluation of AAV9-EF1a-double floxed-hChR2(H134R)-EYFP-WPRE-HGHpA
301 expression in Ucn3 projections from the MePD to the PVN showed YFP labelled fibres in the
302 PVN figure 5, A-Aiii. Local Ucn3 neurons in the PVN are labelled with tdTomato. We cannot
303 however exclude the possibility that a small portion of fibres may be present that are not
304 colocalized with tdTomato, which may reflect unspecific expression of ChR2 in nerve
305 terminals other than Ucn3 in the PVN. The optic fibre cannula was also verified to be correctly
306 positioned in the PVN in all of 8 mice.

307 **Discussion**

308 We show optogenetic stimulation of MePD Ucn3 neurons inhibits pulsatile LH secretion, an
309 effect that was completely blocked by intra-MePD GABA and glutamate antagonism.
310 Moreover, optogenetic stimulation of MePD Ucn3 projections in the hypothalamic PVN also
311 suppresses LH pulsatility while inducing the release of CORT. These results demonstrate that
312 inhibition of the GnRH pulse generator by Ucn3 neurons within the MePD relies on GABA
313 and glutamate signalling in the MePD, *per se*. Moreover, MePD Ucn3 efferent projections in
314 the PVN modulate the activity of the HPA and HPG axes.

315 The MePD is a major upstream regulator of gonadotropic hormone secretion with a significant
316 population of GABAergic neurons projecting to reproductive neural centres in the
317 hypothalamus (26). Although classic lesioning studies suggest an inhibitory output of the
318 MePD over reproductive function (27,28), selective optical stimulation of MePD kiss1 neurons
319 increases LH pulse frequency (4), which our unpublished observations show relies upon both
320 GABA and glutamate signalling in the MePD. Due to this interesting dichotomy, we have
321 proposed a disinhibitory system, which is consistent with the pallidal origin of this limbic
322 structure (29), whereby MePD kiss1 activation excites inhibitory GABAergic interneurons,
323 which in turn reduces the inhibitory tone of the GABAergic projections from the MePD to the

324 ARC KNDy network allowing for an increase in GnRH pulse generator frequency (4).
325 Contrastingly, kiss1R antagonism, reducing MePD kiss1 signalling decreases GnRH pulse
326 generator frequency (30).

327 We have recently shown that stress-induced activation of Ucn3 and CRFR2 signalling within
328 the MePD inhibits GnRH pulse generator activity (3) and activation of MePD Ucn3 neurons
329 delays pubertal timing (31). It has also been shown that the majority of MePD CRFR2
330 expressing neurons are GABAergic (21). In the MePD, Ucn3 fibres overlap with sites
331 expressing its cognate receptor CRFR2 (32,33) and some local Ucn3 neurons within the MePD
332 are shown to have an interneuron-like appearance (34), thus Ucn3 neurons may form
333 connections with and signal via GABAergic CRFR2-positive neurons in this region. In the
334 present study, we show that optogenetic activation of MePD Ucn3 neurons inhibits pulsatile
335 LH secretion. Therefore, we propose that activated MePD Ucn3 neurons may signal through
336 inhibitory GABAergic CRFR2-positive interneurons, upstream to the MePD kiss1 neurons,
337 downregulating MePD kiss1 signalling resulting in decreased GnRH pulse generator
338 frequency, as illustrated in figure 6A.

339 In our proposed model, we hypothesised that GABA signalling is an important factor mediating
340 the suppressive effect of MePD Ucn3 activation on GnRH pulse generator activity. Therefore,
341 we tested the effect of intra-MePD administration of $GABA_A$ or $GABA_B$ receptor antagonists
342 during optical stimulation of MePD Ucn3 neurons on LH pulsatility, and indeed, we found that
343 both $GABA_A$ and $GABA_B$ receptor antagonism blocks the suppression of LH pulses by MePD
344 Ucn3 neuronal activation. Indeed, it has been shown that in $GABA_B$ receptor knock out mice
345 Kiss1 mRNA expression increases in the MePD suggesting $GABA_B$ regulates Kiss1 expression
346 in this region (35). Whether the MePD kiss1 neurons also contain $GABA_A$ receptors is
347 unknown. Selective optical stimulation of Ucn3 neurons may activate inhibitory GABAergic
348 CRFR2-positive interneurons (35), which in turn downregulate MePD kiss1 signalling, which

349 we have previously shown results in suppression of GnRH pulse generator frequency (30) (see
350 Fig. 6A). Although, based on our proposed neuronal circuit, $GABA_A$ and $GABA_B$ receptor
351 antagonism may be working upstream and downstream of MePD kiss1 activity to cancel both
352 the inhibitory GABAergic CRFR2 interneurons upstream to and the inhibitory GABAergic
353 interneurons downstream to MePD kiss1 neurons. Therefore, the inhibitory output of the
354 MePD GABAergic projection neurons to the ARC KNDy network is cancelled, thus, negating
355 the suppressive effect of MePD Ucn3 activation on the GnRH pulse generator. Essentially,
356 terminating the ability of the GABA interneuron, upstream and downstream of MePD kiss1
357 activity, to take part in the disinhibition by antagonising GABA receptors located on the MePD
358 kiss1 neurons as well as post-synaptic GABA projection neurons removing the inhibitory
359 control over the GnRH pulse generator from the MePD (see Fig. 6B).

360 We have identified GABA signalling as a key part of the MePD Ucn3 neural circuitry
361 associated with suppression of the GnRH pulse generator, however glutamate signalling in the
362 amygdala is also known to be involved in modulating reproduction and anxiety-like behaviour
363 (36). Administration of NMDA into the MePD disrupts ovarian cycles in rats, while NMDA
364 receptor antagonism in the MePD delays pubertal timing (28). We hypothesised that glutamate
365 neurotransmission may form a critical part of the MePD Ucn3 neural circuitry involved in
366 stress-induced inhibition of GnRH pulse generator activity. In the present study, we show that
367 intra-MePD AMPA and NMDA receptor antagonism blocks the inhibitory effect of MePD
368 Ucn3 neuronal activation on LH pulsatility. These observations suggest the involvement of
369 similar neural circuitry as in the neighbouring posteroventral medial amygdala which exhibits
370 functional glutamatergic signalling onto inhibitory GABA neurons (29). Moreover, inhibition
371 of both GABA and glutamate signalling is equally effective at blocking suppression of LH
372 pulses suggesting they are key components in the circuit.

373 We know the MePD Ucn3 neurons are interconnected with each other as well as CRFR2
374 expressing neurons, forming a Ucn3-CRFR2 neuronal circuit (21). The effect of glutamate
375 antagonism illustrated in figure 6C, suggests that glutamate transmission may be mediated via
376 glutamatergic Ucn3 neurons. This has been shown in the hypothalamic perifornical area,
377 where they are activated during infant-directed aggression (37) and increase anxiety-like
378 behaviour (38), but this awaits future study for the MePD Ucn3 population. Our previous data
379 shows that infusing Ucn3 in the MePD blocks LH pulses indicating their activity in this brain
380 region is sufficient to suppress GnRH pulse generator activity (3). We have also shown that
381 infusion of CRFR2 antagonists in the MePD blocks the stress-induced suppression of LH
382 pulses suggesting MePD CRFR2 expressing neurons are also involved in modulating the
383 GnRH pulse generator under stressful conditions. Our current data expands on our previous
384 observations determining whether neurotransmission modulating pulsatile LH secretion is
385 involved in this MePD circuit. Our results suggest that glutamate may be necessary for the
386 inhibition of LH pulses induced by activation of MePD Ucn3 neurons, thus we show that
387 glutamate signalling is an indispensable part of this circuit. Based on our observations, we
388 propose that Ucn3 neurons in the MePD may be glutamatergic similarly to the Ucn3 neurons
389 in the hypothalamic perifornical area. Glutamate is possibly required to trigger network
390 activity of the MePD Ucn3 neurons similar to the role glutamate plays in the ARC KNDy
391 network (14). This allows the network to reach a certain level of excitability that promotes
392 signalling via Ucn3 to activate CRFR2 expressing GABAergic neurons, which in turn
393 downregulate MePD kiss1 activity, resulting in suppression of GnRH pulse generator activity.
394 Thus, NMDA and AMPA receptor antagonism possibly cancels MePD Ucn3 glutamatergic
395 activation of inhibitory GABAergic CRFR2 expressing inter-neurons preventing the decrease
396 in GnRH pulse generator activity (Fig. 6C). However, fast synaptic activity occurs due to
397 synaptic neurotransmitter release and modulation of this activity is known to be a key target

398 for neuropeptides. Indeed, urocortins can also function endogenously as modulators of
399 excitatory glutamatergic transmission in the amygdala, with *in vitro* studies showing
400 modulation of glutamatergic excitatory post-synaptic potentials via pre- and postsynaptic
401 CRFR2-mediated mechanisms (39). Therefore, we cannot exclude the possibility that Ucn3
402 activity in the MePD is augmenting glutamatergic transmission to activate downstream
403 inhibitory GABA neurons.

404 The fact that GABAergic and glutamatergic receptor antagonism within the MePD did not alter
405 LH pulsatility without optogenetic stimulation of Ucn3 neurons is an important factor in our
406 proposed mechanisms and neural circuits within the MePD. This observation indicates that
407 under basal non-stress conditions MePD Ucn3 neurons are relatively quiescent, thus solely
408 pharmacologically blocking the upstream GABA and glutamate inputs to the GABAergic
409 MePD projections without a corresponding increase in Ucn3 activity would make little
410 difference to the net effect of the MePD over the KNDy neuronal system.

411 Stress elevates Ucn3 mRNA (19) and c-fos expression in the MePD (18) while chemogenetic
412 inhibition of MePD Ucn3 neurons prevents stress-induced suppression of LH pulsatility (3).
413 The MePD sends stress-activated efferents to the PVN (18) and MePD Ucn3 neurons have
414 been shown to project directly to the PVN (21). In the current study, we demonstrate for the
415 first time that optical stimulation of MePD Ucn3 projections in the PVN inhibits pulsatile LH
416 secretion. Recently, chemogenetic activation of PVN CRF neuron perikarya was shown to
417 rapidly suppress LH pulse frequency, however optogenetic activation of their nerve terminals
418 in the ARC does not affect the firing of KNDy neurons (40) and directly injecting CRF in the
419 ARC also has no effect on LH secretion (41), suggesting the involvement of an indirect
420 mechanism inhibiting GnRH pulse generator activity. The MePD has been shown to send
421 Ucn3 neuronal projections to the PVN and receive Ucn3 projections from the PVN, indicating
422 bidirectional communication between these two brain regions via Ucn3 signalling (21).

423 Moreover, the MePD sends direct efferent projections to KNDy neurons of an unknown
424 neurochemical phenotype (8). Therefore, stressful stimuli may be processed by PVN CRF or
425 Ucn3 neurons and this information may be relayed via the MePD Ucn3 neuronal circuitry to
426 the ARC KNDy neurons to modulate their activity (see Fig. 6D). Ultimately, the MePD may
427 function as a novel relay centre between the PVN and ARC to regulate stress signals to the
428 GnRH pulse generator and contribute to the crosstalk between the reproductive and stress axes.

429 Central administration of Ucn3 augments the HPA axis response to restraint stress in rats (19)
430 and increases hypothalamic CRF concentrations and circulating levels of CORT in mice (42).
431 Overexpression of Ucn3 in the hypothalamic perifornical area increases anxiety-like behaviour
432 (38) and activation of the CRFR2 in the lateral septum is involved in stress-induced persistent
433 anxiety in mice (43). In the medial amygdala, Ucn3 neuronal populations are shown to consist
434 of both projection neurons extending to the PVN, the bed nucleus of the stria terminalis and
435 the suprachiasmatic nucleus (21,34) and local Ucn3 interneurons (32,33). We have previously
436 shown chemogenetic inhibition targeting both local and efferent MePD Ucn3 neurons prevents
437 psychosocial stress-induced release of CORT (3). In the present study, we show that selective
438 optogenetic activation of MePD Ucn3 projections in the PVN elevates CORT secretion, thus
439 MePD Ucn3 projections to the PVN are critical for the regulation of CORT secretion. Further
440 work is required to identify whether only the MePD Ucn3 projecting efferents to the PVN are
441 crucial for regulating CORT secretion. The presence of E_2 is known to up-regulate basal CRF
442 mRNA levels in the PVN in rodents and induce high levels of circulating corticosterone
443 providing a sensitizing effect to the activity of the HPA axis (44,45). Moreover, the CRFR2
444 promoter contains a classical estrogen receptor response element (46), indicating that CRFR2
445 activity is upregulated in the presence of E_2. Therefore, we implanted the OVX mice with E_2
446 capsules for HPA axis sensitization in mice similarly to what has been reported in previous
447 studies (44,47–49). However, E_2 levels may have fallen lower than expected, to low or

448 potentially below the physiological range observed in diestrous mice, as evidenced by little or
449 no effect on LH pulse frequency. However, an effect on LH pulse amplitude and mean LH
450 levels was evident in the E_2 replaced animals (25). Although there was weak E_2 negative
451 feedback on LH pulses in our model, our main reason for E_2 replacement was to sensitizes the
452 HPA axis (44,47–49). PVN-CRF neurons express mRNA transcripts for CRFR2 (50) and
453 CRFR2 primarily activate the Gαs adenylyl cyclase/cAMP signalling pathway (51) indicating
454 that signalling via the CRFR2 located on PVN-CRF neurons may result in activation of this
455 neuronal population and hence the HPA axis (see Fig. 6D). Therefore, Ucn3 released following
456 optical stimulation of MePD Ucn3 projections in the PVN may directly activate the PVN-CRF
457 neurons, signalling via CRFR2, to stimulate CORT release as observed in the present study.
458 However, this hypothesis requires further experimental interrogation.

459 Selective CRFR2 antagonism has been shown to reverse the stress-induced inhibition of LH
460 pulses (52) where central administration of astressin2-B, a specific CRFR2 antagonist, blocked
461 the restraint-stress induced suppression of pulsatile LH secretion in rats (53). We have shown
462 specific antagonism of CRFR2 in the MePD blocked the inhibitory effects of predator odor on
463 the GnRH pulse generator in mice (3) and activation of MePD Ucn3 neurons delayed puberty
464 in mice (31). Therefore, we know CRFR2 neurons are involved in processing stressful
465 information and coordinating the activity of the GnRH pulse generator accordingly.
466 Additionally, CRF is also implicated in reducing pulsatile LH secretion via CRFR1 expressing
467 neurons in mice (54). Chronic stress levels of CORT decrease LH pulsatility (55) and recently
468 an acute rise in CORT sustained for 30-60 min was shown to inhibit pulsatile LH release, but
469 only in OVX mice with estrogen replacement (56) and after a delay of approximately 30 min
470 following the CORT rise. From our observations, inhibition of LH pulsatility occurs
471 immediately after the stimulation of MePD Ucn3 projections in the PVN in OVX E_2 replaced
472 mice, thus it is unlikely the result of negative feedback from CORT release but rather a central

473 suppression of GnRH pulse generator activity possibly from the activation of PVN CRF
474 neurons, although the mechanism involved has yet to be established. Moreover, acute
475 psychosocial stress exposure reduces LH pulse frequency in OVX mice (3,57), suggesting E_2
476 is not necessary for the inhibition of the GnRH pulse generator in response to psychosocial
477 stress (3,57). Therefore, acute stress pathways possibly act via CORT and E_2 independent
478 pathways to suppress LH pulses. In our study, optical stimulation of MePD Ucn3 local and
479 efferent neurons is supposed to mimic acute exposure to psychosocial stress as this has been
480 shown to be processed by Ucn3 activity in the MePD, thus supporting the idea of a central
481 suppression of GnRH pulse generator activity mediated by MePD Ucn3 neurons.

482 The PVN CRF neuronal population was not traditionally considered important for mediating
483 stress-induced suppression of pulsatile LH secretion, as PVN lesion studies have shown that
484 this region is not critical in mediating the stress-induced suppression of the reproductive axis
485 (58). However, with the recent observations showing that chemogenetic activation of PVN
486 CRF neurons indirectly inhibits the GnRH pulse generator it is plausible that the stress neural
487 circuitry includes upstream signalling via the MePD. Therefore, a possible route may involve
488 stressful information processed by the PVN CRF neurons relayed via the MePD Ucn3 neuronal
489 circuitry to the ARC KNDy neurons to modulate their activity (see Fig. 6D). The neighbouring
490 central nucleus of the amygdala is known to act as a relay centre in pain control where the
491 central lateral part receives nociceptive input from the parabrachial nucleus and the central
492 medial part is involved in regulating the output of defensive behaviour and nociception (59).
493 Local and efferent MePD Ucn3 signalling plays a critical dual role in regulating GnRH pulse
494 generator activity and CORT secretion, thus MePD Ucn3 neuronal populations and their
495 projections may represent a novel nodal centre in the interaction between the reproductive and
496 stress axes.

497 Our findings show for the first time that stimulation of local Ucn3 neurons in the MePD inhibits
498 GnRH pulse generator activity involving an interplay between Ucn3, GABA and glutamate
499 signalling within the MePD. Furthermore, we interrogate the MePD Ucn3 neuron projection
500 terminals in the PVN demonstrating that stimulation of the MePD Ucn3 efferent projections in
501 the PVN elevates CORT secretion to stress levels while suppressing the GnRH pulse generator.
502 How the local neural circuit within the MePD engages with efferent projections from the MePD
503 to the PVN and the interplay between Ucn3, GABA and glutamate neurons to mediate the
504 suppressive effect on LH pulsatility and the stimulatory effect on the HPA axis remains an
505 exciting question for the future.

506 **Bibliography**

507 1. Ressler KJ. Amygdala Activity, Fear, and Anxiety: Modulation by Stress. Biol
508 Psychiatry. 2010;67(12):1117–9.

509 2. Lin Y, Li XF, Lupi M, Kinsey-Jones JS, Shao B, Lightman SL, O'Byrne KT . The role
510 of the medial and central amygdala in stress-induced suppression of pulsatile LH
511 secretion in female rats. Endocrinology. 2011;152(2):545–55.

512 3. Ivanova D, Li XF, McIntyre C, Liu Y, Kong L, O'Byrne KT . Urocortin3 in the
513 Posterodorsal Medial Amygdala Mediates Stress-induced Suppression of LH
514 Pulsatility in Female Mice. Endocrinology. 2021;162(12):bqab206.

515 4. Lass G, Li XF, de Burgh RA, He W, Kang Y, Hwa-Yeo S, Sinnett-Smith LC,
516 Manchishi SM, Colledge WH, Lightman SL, O'Byrne KT . Optogenetic stimulation of
517 kisspeptin neurones within the posterodorsal medial amygdala increases luteinising
518 hormone pulse frequency in female mice. J Neuroendocrinol. 2020;32(2):e12823.

519 5. Li XF, Adekunbi DA, Alobaid HM, Li S, Pilot M, Lightman SL, O'Byrne KT . Role
520 of the posterodorsal medial amygdala in predator odour stress-induced puberty delay

521 in female rats. J Neuroendocrinol. 2019;31(6):e12719.

522 6. Adekunbi DA, Li XF, Li S, Adegoke OA, Iranloye BO, Morakinyo AO, Lightman SL,
523 Taylor PD, Poston L, O'Byrne KT . Role of amygdala kisspeptin in pubertal timing in
524 female rats. PLoS One. 2017;12(8):e0183596.

525 7. Moore AM, Coolen LM, Lehman MN. Kisspeptin/Neurokinin B/Dynorphin (KNDy)
526 cells as integrators of diverse internal and external cues: evidence from viral-based
527 monosynaptic tract-tracing in mice. Sci Rep. 2019;9(1):1–5.

528 8. Yeo SH, Kyle V, Blouet C, Jones S, Colledge WH. Mapping neuronal inputs to Kiss1
529 neurons in the arcuate nucleus of the mouse. PLoS One. 2019;14(3):e0213927.

530 9. Qiu J, Nestor CC, Zhang C, Padilla SL, Palmiter RD, Kelly MJ, Rønnekleiv OK .
531 High-frequency stimulation-induced peptide release synchronizes arcuate kisspeptin
532 neurons and excites GnRH neurons. Elife. 2016;5:e16246.

533 10. Clarkson J, Han SY, Piet R, McLennan T, Kane GM, Ng J, Porteous RW, Kim JS,
534 Colledge WH, Iremonger KJ, Herbison AE . Definition of the hypothalamic GnRH
535 pulse generator in mice. Proc Natl Acad Sci U S A. 2017;114(47):e10216–23.

536 11. Voliotis M, Li XF, De Burgh R, Lass G, Lightman SL, O'Byrne KT, Tsaneva-
537 Atanasova K . The Origin of GnRH pulse generation: An integrative mathematical-
538 experimental approach. J Neurosci. 2019;39(49):9738–47.

539 12. Moore AM, Coolen LM, Lehman MN. In vivo imaging of the GnRH pulse generator
540 reveals a temporal order of neuronal activation and synchronization during each pulse.
541 Proc Natl Acad Sci U S A. 2022;119(6).

542 13. Han SY, McLennan T, Czieselsky K, Herbison AE. Selective optogenetic activation of
543 arcuate kisspeptin neurons generates pulsatile luteinizing hormone secretion. Proc Natl
544 Acad Sci U S A. 2015;112(42):13109–14.

545 14. Voliotis M, Li XF, De Burgh RA, Lass G, Ivanova D, McIntyre C, O'Byrne K,
546 Tsaneva-Atanasova K . Modulation of pulsatile GnRH dynamics across the ovarian
547 cycle via changes in the network excitability and basal activity of the arcuate
548 kisspeptin network. Elife. 2021;10.

549 15. Martin EI, Ressler KJ, Binder E, Nemeroff CB. The Neurobiology of Anxiety
550 Disorders: Brain Imaging, Genetics, and Psychoneuroendocrinology. Psychiatr Clin
551 North Am. 2009;32(3):549.

552 16. Nuss P. Anxiety disorders and GABA neurotransmission: A disturbance of
553 modulation. Neuropsychiatr Dis Treat. 2015;11:165–75.

554 17. Takahashi LK. Olfactory systems and neural circuits that modulate predator odor fear.
555 Front Behav Neurosci. 2014;8:72.

556 18. Van-Hover C, Li C. Stress-activated afferent inputs into the anterior parvicellular part
557 of the paraventricular nucleus of the hypothalamus: Insights into urocortin 3 neuron
558 activation. Brain Res. 2015;1611:29–43.

559 19. Jamieson PM, Li C, Kukura C, Vaughan J, Vale W. Urocortin 3 modulates the
560 neuroendocrine stress response and is regulated in rat amygdala and hypothalamus by
561 stress and glucocorticoids. Endocrinology. 2006;147(10):4578–88.

562 20. Fekete ÉM, Zhao Y, Li C, Sabino V, Vale WW, Zorrilla EP. Social defeat stress
563 activates medial amygdala cells that express type 2 corticotropin-releasing factor
564 receptor mRNA. Neuroscience. 2009;162(1):5–13.

565 21. Shemesh Y, Forkosh O, Mahn M, Anpilov S, Sztainberg Y, Manashirov S,
566 Shlapobersky T, Elliott E, Tabouy L, Ezra G, Adler ES . Ucn3 and CRF-R2 in the
567 medial amygdala regulate complex social dynamics. Nat Neurosci. 2016;19(11):1489–
568 96.

569 22. Ingberg E, Theodorsson A, Theodorsson E, Strom JO . Methods for long-term 17β-
570 estradiol administration to mice. Gen Comp Endocrinol. 2012;175(1):188–93.

571 23. Paxinos G, Franklin KB . Mouse Brain in Stereotaxic Coordinates. Acad Press.
572 2019;5:246.

573 24. McCosh RB, Kreisman MJ, Breen KM. Frequent tail-tip blood sampling in mice for
574 the assessment of pulsatile luteinizing hormone secretion. J Vis Exp. 2018;(137).

575 25. Ivanova D. Supplementary Data. OSF. 2022;September. osf.io/vem8y

576 26. Pardo-Bellver C, Cádiz-Moretti B, Novejarque A, Martínez-García F, Lanuza E.
577 Differential efferent projections of the anterior, posteroventral, and posterodorsal
578 subdivisions of the medial amygdala in mice. Front Neuroanat. 2012;6(33):1–26.

579 27. Stephens SBZ, Raper J, Bachevalier J, Wallen K. Neonatal amygdala lesions advance
580 pubertal timing in female rhesus macaques. Psychoneuroendocrinology. 2015;51:307–
581 17.

582 28. Li XF, Hu MH, Hanley BP, Lin YS, Poston L, Lightman SL, O'Byrne KT . The
583 posterodorsal medial amygdala regulates the timing of puberty onset in female rats.
584 Endocrinology. 2015;156(10):3725–36.

585 29. Keshavarzi S, Sullivan RKP, Ianno DJ, Sah P. Functional properties and projections of
586 neurons in the medial amygdala. J Neurosci. 2014;34(26):8699–715.

587 30. Comninos AN, Anastasovska J, Sahuri-Arisoylu M, Li XF, Li S, Hu M, Jayasena CN,
588 Ghatei MA, Bloom SR, Matthews PM, O'Byrne KT . Kisspeptin signaling in the
589 amygdala modulates reproductive hormone secretion. Brain Struct Funct.
590 2016;221(4):2035–47.

591 31. Ivanova D, Li X, Liu Y, McIntyre C, Fernandes C, Lass G, Kong L, O'Byrne KT .
592 Role of Posterodorsal Medial Amygdala Urocortin-3 in Pubertal Timing in Female

593 Mice. Front Endocrinol (Lausanne). 2022;0:910.

594 32. Cavalcante JC, Sita LV, Mascaro MB, Bittencourt JC, Elias CF. Distribution of
595 urocortin 3 neurons innervating the ventral premammillary nucleus in the rat brain.
596 Brain Res. 2006;1089(1):116–25.

597 33. Li C, Vaughan J, Sawchenko PE, Vale WW. Urocortin III-immunoreactive projections
598 in rat brain: Partial overlap with sites of type 2 corticotrophin-releasing factor receptor
599 expression. J Neurosci. 2002;22(3):991–1001.

600 34. Deussing JM, Breu J, Kühne C, Kallnik M, Bunck M, Glasl L, Yen YC, Schmidt MV,
601 Zurmühlen R, Vogl AM, Gailus-Durner V . Urocortin 3 modulates social
602 discrimination abilities via corticotropin-releasing hormone receptor type 2. J
603 Neurosci. 2010;30(27):9103–16.

604 35. Di Giorgio NP, Semaan SJ, Kim J, López PV, Bettler B, Libertun C, Lux-Lantos VA,
605 Kauffman AS . Impaired GABAB receptor signaling dramatically up-regulates Kiss1
606 expression selectively in nonhypothalamic brain regions of adult but not prepubertal
607 mice. Endocrinology. 2014;155(3):1033–44.

608 36. Hegoburu C, Parrot S, Ferreira G, Mouly AM. Differential involvement of amygdala
609 and cortical NMDA receptors activation upon encoding in odor fear memory. Learn
610 Mem. 2014;21(12):651–5.

611 37. Autry AE, Wu Z, Kapoor V, Kohl J, Bambah-Mukku D, Rubinstein ND, Marin-
612 Rodriguez B, Carta I, Sedwick V, Tang M, Dulac C . Urocortin-3 neurons in the
613 mouse perifornical area promote infant-directed neglect and aggression. Elife.
614 2021;10.

615 38. Kuperman Y, Issler O, Regev L, Musseri I, Navon I, Neufeld-Cohen A, Gil S, Chen A
616 . Perifornical urocortin-3 mediates the link between stress-induced anxiety and energy

617 homeostasis. Proc Natl Acad Sci U S A. 2010;107(18):8393–8.

618 39. Liu J, Yu B, Neugebauer V, Grigoriadis DE, Rivier J, Vale WW, Shinnick-Gallagher
619 P, Gallagher JP . Corticotropin-releasing factor and Urocortin I modulate excitatory
620 glutamatergic synaptic transmission. J Neurosci. 2004;24(16):4020–9.

621 40. Yip SH, Liu X, Hessler S, Cheong I, Porteous R, Herbison AE. Indirect Suppression of
622 Pulsatile LH Secretion by CRH Neurons in the Female Mouse. Endocrinology.
623 2021;162(3).

624 41. Rivest S, Plotsky PM, Rivier C. CRF alters the infundibular LHRH secretory system
625 from the medial preoptic area of female rats: possible involvement of opioid receptors.
626 Neuroendocrinology. 1993;57(2):236–46.

627 42. Bagosi Z, Csabafi K, Karasz G, Jászberényi M, Földesi I, Siska A, Szabó G, Telegdy
628 G . The effects of the urocortins on the hypothalamic-pituitary-adrenal axis -
629 similarities and discordancies between rats and mice. Peptides. 2019;112:1–13.

630 43. Anthony TE, Dee N, Bernard A, Lerchner W, Heintz N, Anderson DJ. Control of
631 stress-induced persistent anxiety by an extra-amygdala septohypothalamic circuit.
632 Cell. 2014;156(3):522–36.

633 44. Li XF, Mitchell JC, Wood S, Coen CW, Lightman SL, O'Byrne KT . The effect of
634 oestradiol and progesterone on hypoglycaemic stress-induced suppression of pulsatile
635 luteinizing hormone release and on corticotropin-releasing hormone mRNA expression
636 in the rat. J Neuroendocrinol. 2003;15(5):468–76.

637 45. Zavala E, Voliotis M, Zerenner T, Tabak J, Walker JJ, Li XF, Terry JR, Lightman SL,
638 O'byrne K, Tsaneva-Atanasova K . Dynamic Hormone Control of Stress and Fertility.
639 Front Physiol. 2020;11:1457.

640 46. Catalano RD, Kyriakou T, Chen J, Easton A, Hillhouse EW. Regulation of

641 Corticotropin-Releasing Hormone Type 2 Receptors by Multiple Promoters and
642 Alternative Splicing: Identification of Multiple Splice Variants. Mol Endocrinol.
643 2003;17(3):395–410.

644 47. Cagampang FR, Cates PS, Sandhu S, Strutton PH, McGarvey C, Coen CW, O'Byrne
645 KT . Hypoglycaemia-induced inhibition of pulsatile luteinizing hormone secretion in
646 female rats: role of oestradiol, endogenous opioids and the adrenal medulla. J
647 Neuroendocrinol. 1997;9(11):867–72.

648 48. Chen MD, O'Byrne KT, Chiappini SE, Hotchkiss J, Knobil E . Hypoglycemic "stress"
649 and gonadotropin-releasing hormone pulse generator activity in the rhesus monkey:
650 role of the ovary. Neuroendocrinology. 1992;56(5):666–73.

651 49. McCosh RB, Breen KM, Kauffman AS . Neural and Endocrine Mechanisms
652 Underlying Stress-Induced Suppression of Pulsatile LH Secretion. Mol Cell
653 Endocrinol. 2019;498:110579.

654 50. Dabrowska J, Hazra R, Guo JD, DeWitt S, Rainnie DG. Central CRF neurons are not
655 created equal: Phenotypic differences in CRF-containing neurons of the rat
656 paraventricular hypothalamus and the bed nucleus of the stria terminalis. Front
657 Neurosci. 2013;0(7 AUG):156.

658 51. Deussing JM, Chen A. The corticotropin-releasing factor family: Physiology of the
659 stress response. Vol. 98, Physiological Reviews. 2018. p. 2225–86.

660 52. Li XF, Bowe JE, Kinsey-Jones JS, Brain SD, Lightman SL, O'Byrne KT . Differential
661 role of corticotropin-releasing factor receptor types 1 and 2 in stress-induced
662 supression of pulsatile luteinising hormone secretion in the female rat. J
663 Neuroendocrinol. 2006;18(8):602–10.

664 53. Li XF, Bowe JE, Lightman SL, O'Byrne KT . Role of corticotropin-releasing factor

665 receptor-2 in stress-induced suppression of pulsatile luteinizing hormone secretion in
666 the rat. Endocrinology. 2005;146(1):318–22.

667 54. Raftogianni A, Roth LC, García-González D, Bus T, Kühne C, Monyer H, Spergel DJ,
668 Deussing JM, Grinevich V . Deciphering the Contributions of CRH Receptors in the
669 Brain and Pituitary to Stress-Induced Inhibition of the Reproductive Axis. Front Mol
670 Neurosci. 2018;11:305.

671 55. Kreisman MJ, McCosh RB, Tian K, Song CI, Breen KM. Estradiol Enables Chronic
672 Corticosterone to Inhibit Pulsatile Luteinizing Hormone Secretion and Suppress Kiss1
673 Neuronal Activation in Female Mice. Neuroendocrinology. 2020;110(6):501–16.

674 56. Kreisman MJ, McCosh RB, Breen KM . Role of CORT Duration and Estradiol
675 Dependence for Stress-level of CORT to Inhibit Pulsatile LH Secretion in Female
676 Mice. J Endocr Soc. 2021;Apr;5(Supplement_1):A552-.

677 57. Yang JA, Song CI, Hughes JK, Kreisman MJ, Parra RA, Haisenleder DJ, Kauffman
678 AS, Breen KM . Acute psychosocial stress inhibits LH pulsatility and kiss1 neuronal
679 activation in female mice. Endocrinology. 2017;158(11):3716–23.

680 58. Serge S, Rivier C. Influence of the paraventricular nucleus of the hypothalamus in the
681 alteration of neuroendocrine functions induced by intermittent footshock or
682 interleukin. Endocrinology. 1991;129(4):2049–58.

683 59. Wank I, Pliota P, Badurek S, Kraitsy K, Kaczanowska J, Griessner J, Kreitz S, Hess A,
684 Haubensak W . Central amygdala circuitry modulates nociceptive processing through
685 differential hierarchical interaction with affective network dynamics. Commun Biol.
686 2021;4(1):1–10.

687

688 **Figure 1.** Optogenetic stimulation of posterodorsal medial amygdala (MePD) urocortin-3

689 (Ucn3) neurons with blue light at 10 Hz, 10 mW suppressed pulsatile LH secretion in adult
690 ovariectomised (OVX) Ucn3-cre-tdTomato female mice. Infusion of bicuculline (BIC),
691 $GABA_A$ receptor antagonist, CGP, $GABA_B$ receptor antagonist, and AP5 and CNQX, NMDA
692 and AMPA receptor antagonists, respectively, into the posterodorsal medial amygdala (MePD)
693 during optogenetic stimulation of MePD urocortin-3 (Ucn3) neurons with blue light at 10 Hz,
694 10 mW completely blocked the suppressive effect of MePD Ucn3 neuronal activation on LH
695 pulsatility. Representative LH pulse profiles showing the effects of (A) control AAV-YFP
696 mice administered with aCSF receiving optical stimulation of 10 Hz, 10 mW, (B) AAV-ChR2
697 mice administered with aCSF receiving optical stimulation of 10 Hz, 10 mW, (C) Summary of
698 LH pulse interval for the pre-stimulation control period (1 h) and optical stimulation/infusion
699 period (1 h), (D) AAV-ChR2 mice administered with BIC, (E) AAV-ChR2 mice administered
700 with BIC receiving optical stimulation of 10 Hz, 10 mW, (F) Summary of LH pulse interval,
701 (G) AAV-ChR2 mice administered with CGP, (H) AAV-ChR2 mice administered with CGP
702 receiving optical stimulation of 10 Hz, 10 mW, (I) Summary of LH pulse interval, (J) AAV-
703 ChR2 mice administered with a combination of AP5 and CNQX, (K) AAV-ChR2 mice
704 administered with a combination of AP5 and CNQX receiving optical stimulation of 10 Hz, 10
705 mW, (L) Summary of LH pulse interval. LH pulses detected by the DynePeak algorithm are
706 indicated with an asterisk located above each pulse on the representative LH pulse profiles. For
707 A-C +++$p<0.0001$ control period vs optic stimulation + aCSF (AAV-ChR2: n = 9); ##$p<0.001$
708 optic stimulation vs control group (AAV-YFP: n = 3; no stimulation: n = 2). For D-F n = 8-9
709 per group. For G-I n = 7 per group. For J-L n = 6 per group.

710 **Figure 2.** Optogenetic stimulation of posterodorsal medial amygdala (MePD) urocortin-3
711 (Ucn3) neuronal terminals in the hypothalamic paraventricular nucleus (PVN) with blue light
712 at 20 Hz, 15 mW elevated corticosterone (CORT) secretion in adult ovariectomised (OVX) +
713 17ß-estradiol (E_2) Ucn3-cre-tdTomato female mice. CORT secretion time-course for mice

714 receiving optical stimulation initiated at 0 min and terminated at 60 min (1 h duration),
715 followed by a 1 h recovery period (60-120 min) for the AAV-ChR2 group (blue line, circles)
716 and control group (red line, squares). +p<0.05 AAV-ChR2 (n = 6) at time point 30 min and
717 60 min vs. control (AAV-YFP: n = 5) at time point 30 min and 60 min.

718 **Figure 3.** Optogenetic stimulation of posterodorsal medial amygdala (MePD) urocortin-3
719 (Ucn3) neuronal terminals in the hypothalamic paraventricular nucleus (PVN) with blue light
720 at 20 Hz, 15 mW reduced LH pulsatility in adult ovariectomised (OVX) + 17ß-estradiol (E_2)
721 Ucn3-cre-tdTomato female mice. Representative LH pulse profiles showing the effects of (A)
722 AAV-YFP/WT mice receiving optical stimulation of 20 Hz, 5 mW, (B) AAV-ChR2 mice
723 receiving optical stimulation of 20 Hz, 5 mW, (C) Another example of AAV-YFP/WT mice
724 receiving optical stimulation of 20 Hz, 5 mW, (D) Another example of AAV-ChR2 mice
725 receiving optical stimulation of 20 Hz, 5 mW, (E) Summary of LH pulse interval for the pre-
726 stimulation control period (1 h) and optic stimulation period (1 h). LH pulses detected by the
727 DynePeak algorithm are indicated with an asterisk located above each pulse on the
728 representative LH pulse profiles. +++p<0.0001 control period vs optic stimulation for AAV-
729 ChR2 mice (n = 8); ###p<0.0001 AAV-YFP/WT (AAV-YFP, n = 3; wild-type with AAV-
730 ChR2, n = 2; no stimulation, n = 2) vs AAV-ChR2 mice during optic stimulation.

731 **Figure 4.** Expression of AAV9-EF1a-double floxed-hChR2(H134R)-EYFP-WPRE-HGHpA
732 in posterodorsal medial amygdala (MePD) Urocortin-3 (Ucn3) neurons. (A-E) Representative
733 dual fluorescence photomicrographs of the MePD from a Ucn3-cre-tdTomato female
734 ovariectomised (OVX) mouse injected with AAV9-EF1a-double floxed-hChR2(H134R)-
735 EYFP-WPRE-HGHpA. Ucn3 neurons labelled with tdTomato (A) and YFP (C) appear
736 yellow/orange (E). (B), (D) and (F) are a higher power view of (A), (C) and (E) respectively.
737 Scale bars represent A, C, E 50 μm and B, D, F 20 μm. White arrows show examples of Ucn3

738 neurons labelled with tdTomato and YFP. OT, Optic tract (blue line).

739 **Figure 5.** Expression of AAV9-EF1a-double floxed-hChR2(H134R)-EYFP-WPRE-HGHpA
740 in Urocortin-3 (Ucn3) neuronal projection in the paraventricular nucleus of the hypothalamus
741 (PVN) originating from the posterodorsal medial amygdala (MePD). (A-Aiii) Representative
742 dual fluorescence photomicrographs of the PVN from a Ucn3-cre-tdTomato female
743 ovariectomised (OVX) + 17ß-estradiol (E_2) mouse injected with AAV9-EF1a-double floxed-
744 hChR2(H134R)-EYFP-WPRE-HGHpA. Ucn3 neurons and projections labelled with (A) YFP
745 and tdTomato expression in PVN, (Ai) higher power view of YFP labelled MePD Ucn3
746 projections in the PVN, (Aii) higher power view of tdTomato labelled MePD Ucn3 projections
747 in the PVN and (Aiii) YFP and tdTomato merged. Scale bars represent A, 100 μm, Ai, Aii and
748 Aiii, 10 μm. Blue box shows the YFP labelled MePD Ucn3 projections in the PVN, yellow
749 arrows point to parts of the YFP labelled MePD Ucn3 projection in the PVN. 3V; third
750 ventricle.

751 **Figure 6.** Schematic illustration of the MePD neurocircuits and their pharmacological
752 manipulation. (A) Optical stimulation of local MePD Ucn3 neurons releases Ucn3 and the co-
753 transmitter glutamate, which activate inhibitory GABAergic CRFR2-positive interneurons
754 located upstream to the kiss1 neurons suppressing their activity. The reduced kiss1 signalling
755 deactivates its downstream inhibitory GABAergic interneuron causing disinhibition of the
756 GABAergic projection efferents from the MePD, resulting in an increased inhibitory tone over
757 the ARC KNDy network, thus decreasing GnRH pulse generator frequency. (B) Antagonism
758 of both $GABA_A$ and $GABA_B$ receptors in the MePD during optical stimulation of Ucn3 neurons
759 blocks the downregulation of kiss1 neuronal activity, preventing the inhibitory effect of Ucn3
760 signalling on the KNDy network. (C) Antagonism of both NMDA and AMPA receptors in
761 the MePD during optical stimulation of Ucn3 neurons blocks the activation of the downstream

762 GABAergic CRFR2-positive interneurons, preventing the inhibitory effect of Ucn3 signalling
763 on the KNDy network and suggesting glutamate is necessary for the inhibition of pulsatile LH
764 secretion. (D) High frequency photoactivation of MePD Ucn3 projection terminals in the PVN
765 may activate Ucn3 neurons and/or other neurons of an unknown phenotype in the PVN
766 resulting in stimulation of the HPA axis and CORT release. Additionally, there may be
767 collateral activation of reciprocal PVN Ucn3 projections to the MePD, which in turn relay via
768 the MePD Ucn3 neuronal circuitry an inhibitory influence on the ARC KNDy neuronal
769 network to suppress GnRH pulse generator frequency. Urocortin3 (Ucn3), Corticotropin-
770 releasing factor type 2 receptor (CRFR2), glutamate receptor (GlutR), the posterodorsal
771 subnucleus of the medial amygdala (MePD), paraventricular nucleus of hypothalamus (PVN),
772 the hypothalamic arcuate nucleus (ARC).

Figure 1

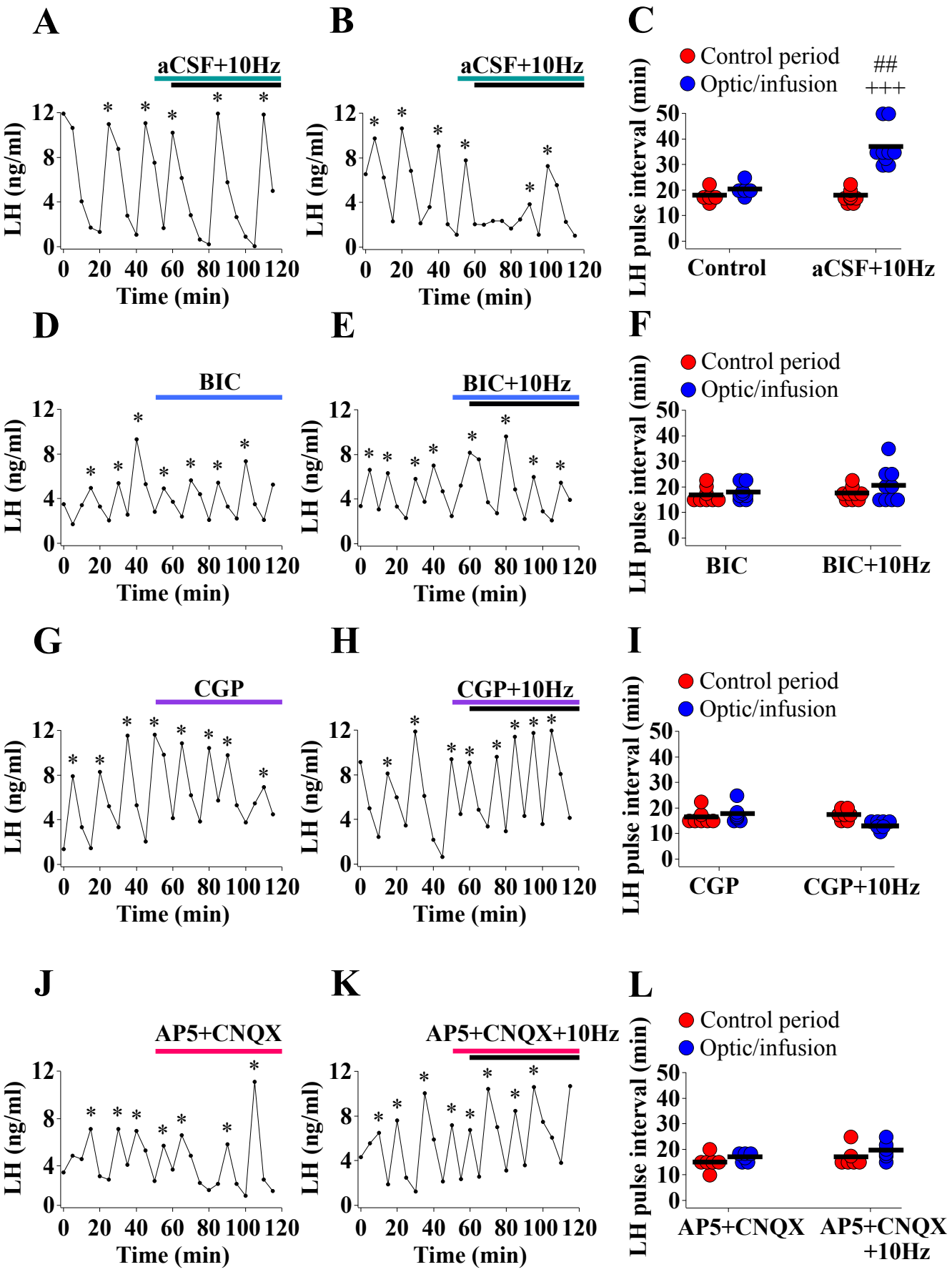
A
aCSF+10Hz
LH (ng/ml)
Time (min)
B
aCSF+10Hz
LH (ng/ml)
Time (min)
C
Control period
Optic/infusion
##
+++
LH pulse interval (min)
Control
aCSF+10Hz
D
BIC
LH (ng/ml)
Time (min)
E
BIC+10Hz
LH (ng/ml)
Time (min)
F
Control period
Optic/infusion
LH pulse interval (min)
BIC
BIC+10Hz
G
CGP
LH (ng/ml)
Time (min)
H
CGP+10Hz
LH (ng/ml)
Time (min)
I
Control period
Optic/infusion
LH pulse interval (min)
CGP
CGP+10Hz
J
AP5+CNQX
LH (ng/ml)
Time (min)
K
AP5+CNQX+10Hz
LH (ng/ml)
Time (min)
L
Control period
Optic/infusion
LH pulse interval (min)
AP5+CNQX
AP5+CNQX
+10Hz

Figure 2

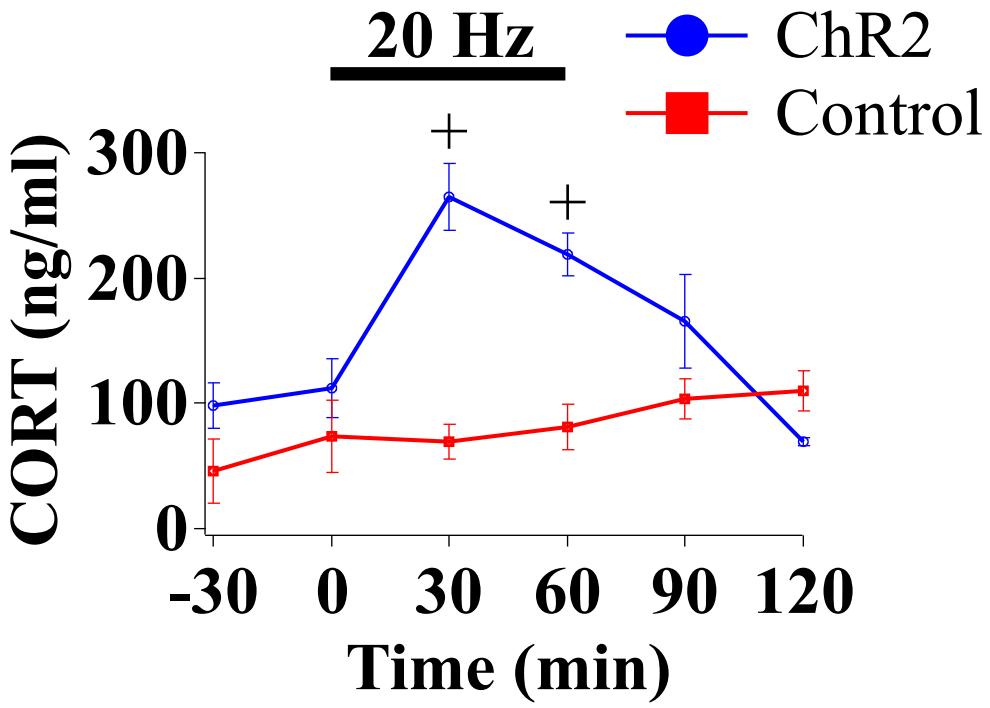
20 Hz
ChR2
Control
CORT (ng/ml)
300
200
100
0
-30
0
30
60
90
120
Time (min)

Figure 3

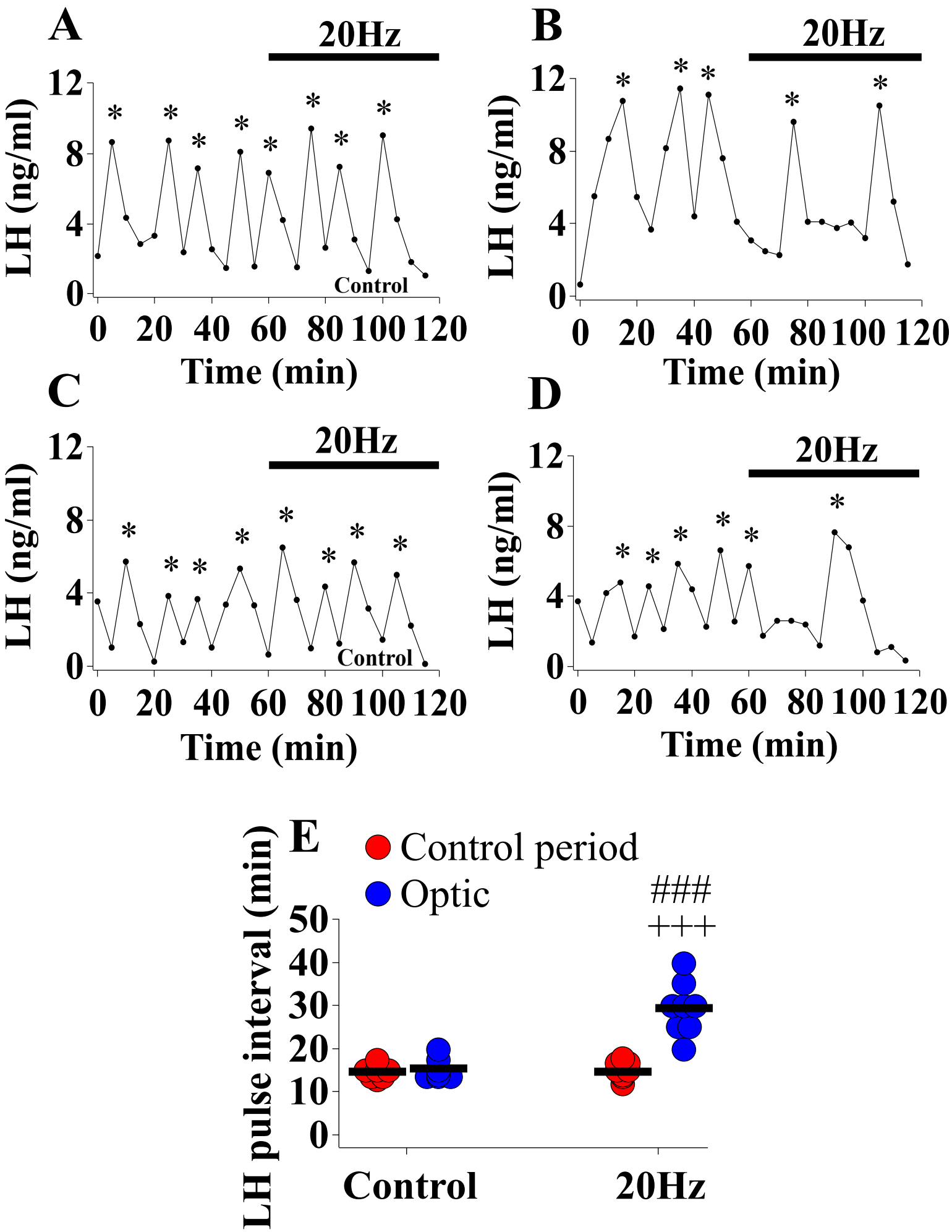
A
20Hz
LH (ng/ml)
Control
Time (min)
B
20Hz
LH (ng/ml)
Time (min)
C
20Hz
LH (ng/ml)
Control
Time (min)
D
20Hz
LH (ng/ml)
Time (min)
E
Control period
Optic
###
+++
LH pulse interval (min)
Control
20Hz

Figure 4

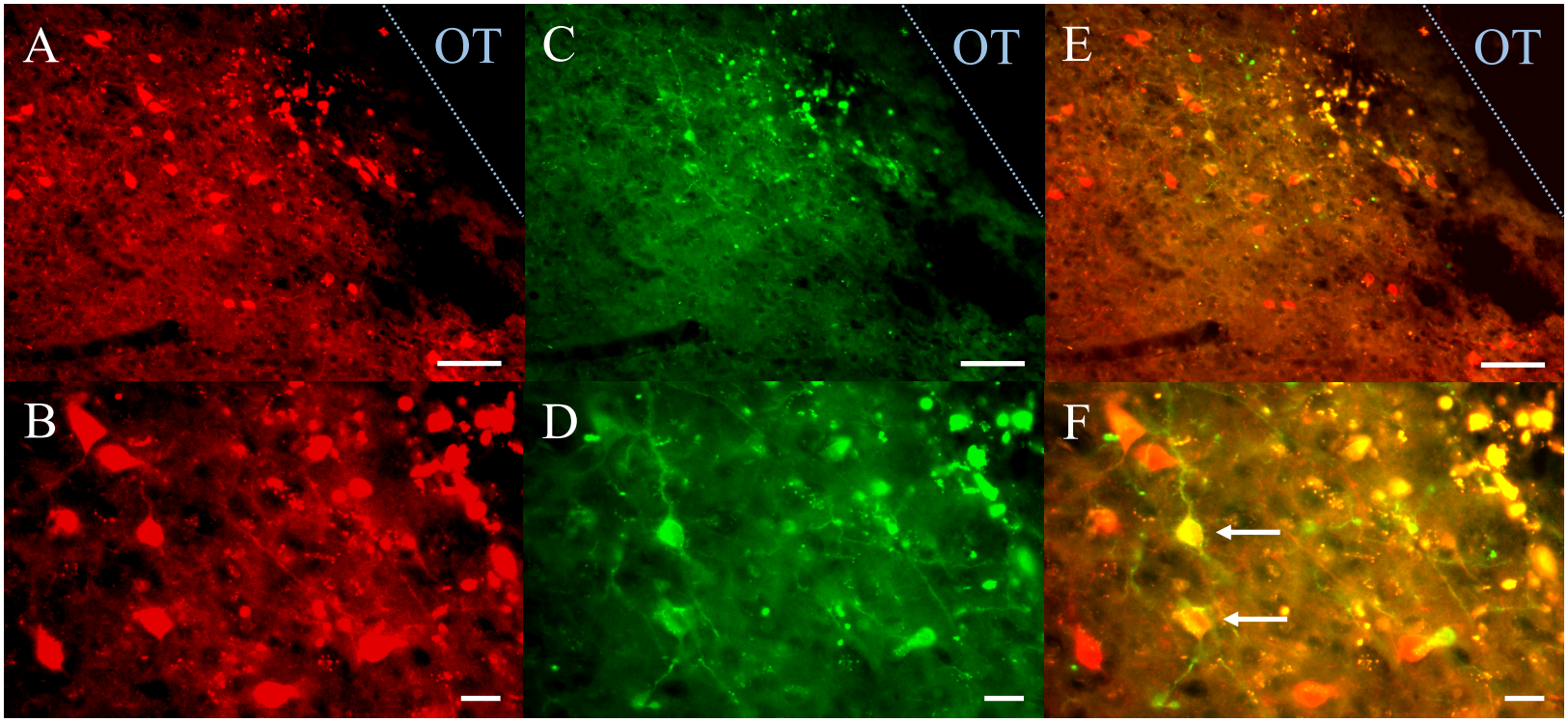

Figure 5

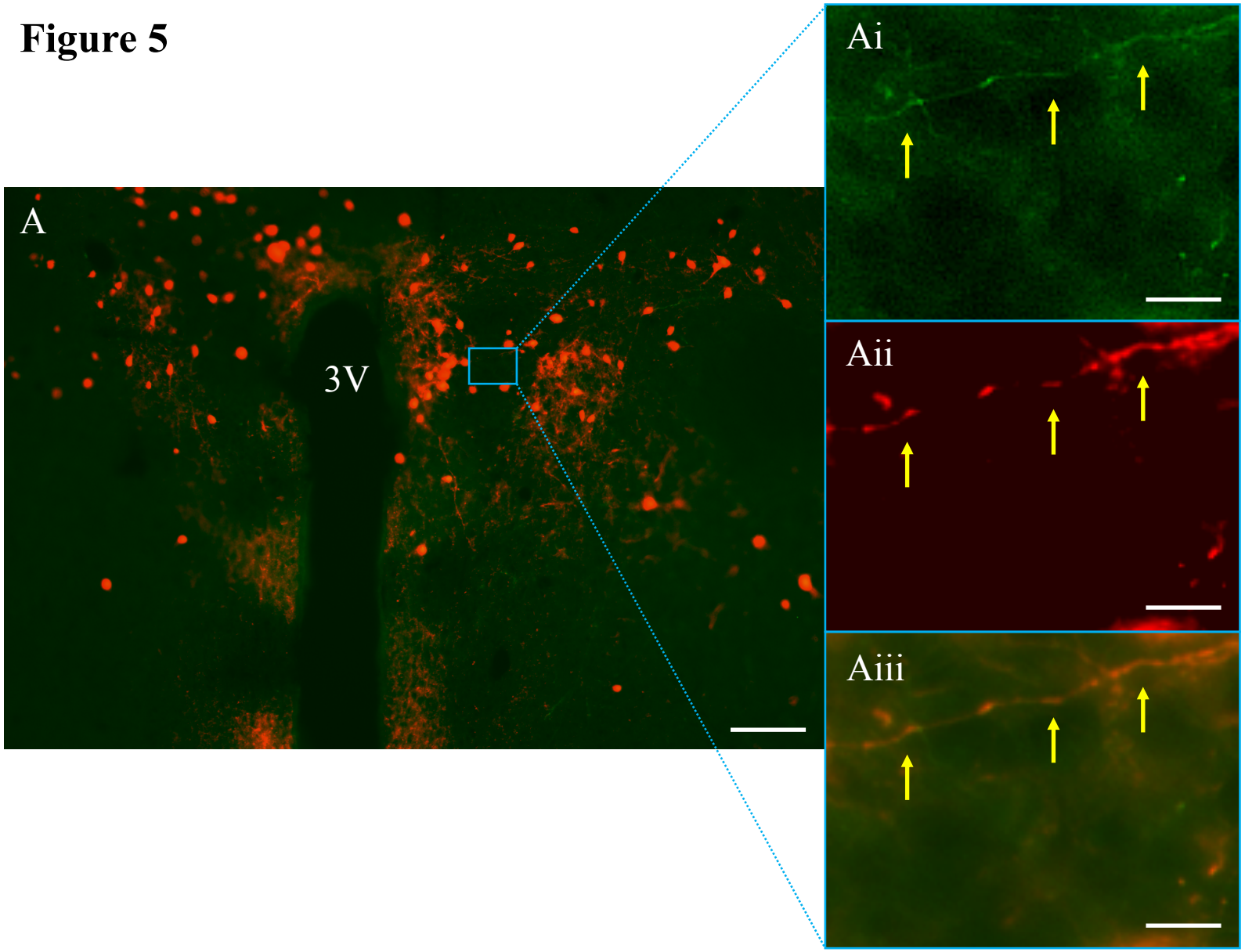

Figure 6

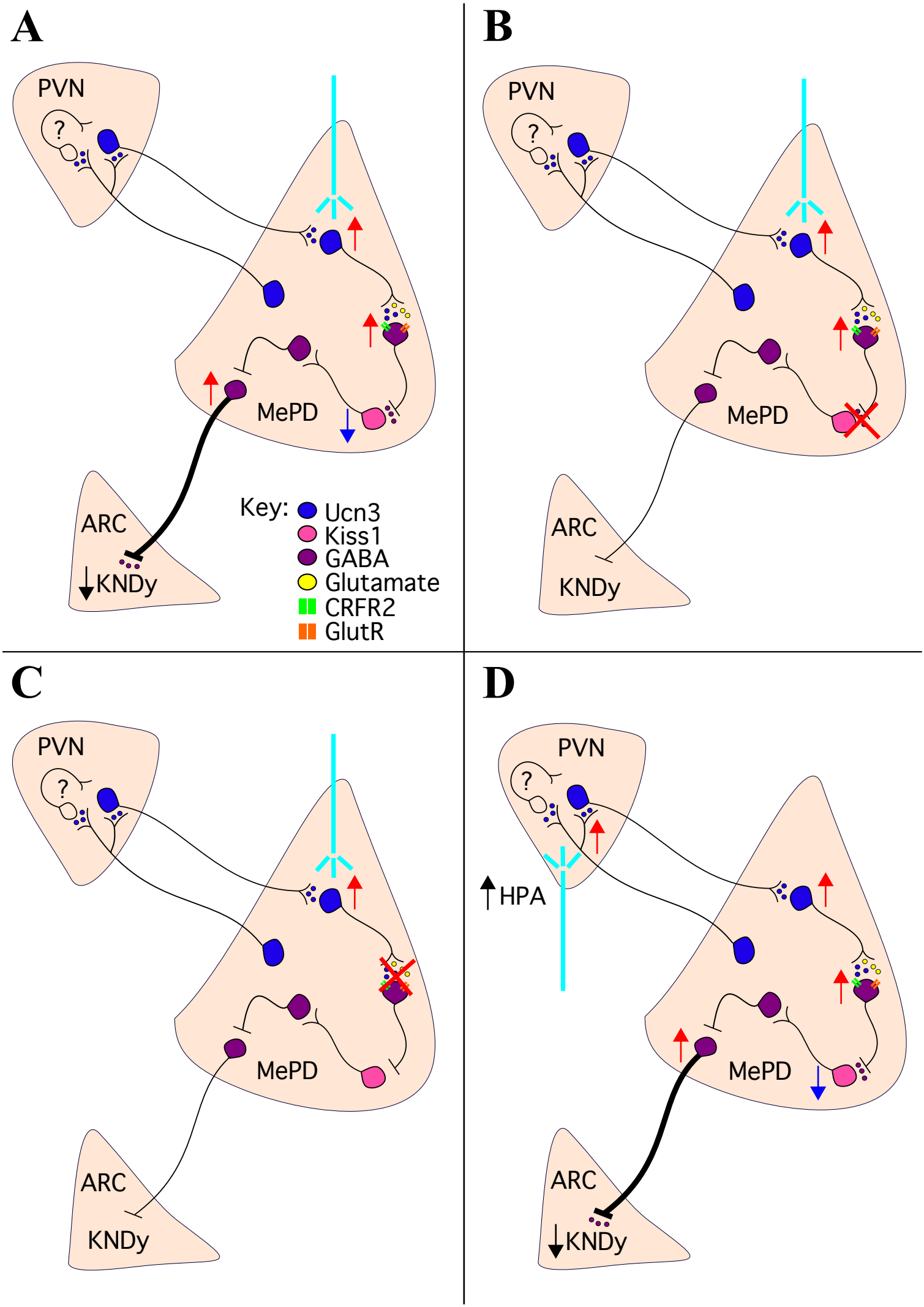
A
PVN
?
MePD
ARC
KNDy
Key:
Ucn3
Kiss1
GABA
Glutamate
CRFR2
GlutR
B
PVN
?
MePD
ARC
KNDy
C
PVN
?
MePD
ARC
KNDy
D
PVN
?
HPA
MePD
ARC
KNDy